Slow highly charged ion induced nanopit formation on the KCl(001) surface

Wilhelm, R. A.; Heller, R.; Facsko, S.;

Originally published:

September 2016

EPL - Europhysics Letters 115(2016), 43001

DOI: https://doi.org/10.1209/0295-5075/115/43001

Perma-Link to Publication Repository of HZDR:

https://www.hzdr.de/publications/Publ-23731

Slow highly charged ion induced nanopit formation on the KCl(001) surface

R.A. Wilhelm[1], R. Heller[1] and S. Facsko[1]

[1] *Helmholtz-Zentrum Dresden-Rossendorf, Institute of Ion Beam Physics and Materials Research, Bautzner Landstr. 400, 01328 Dresden, Germany*

PACS 34.35.+a – Interactions of atoms and molecules with surfaces
PACS 61.72.J- – Point defects and defect clusters
PACS 79.20.Rf – Atomic, molecular, and ion beam impact and interactions with surfaces

Abstract –We report on nanostructuring of the KCl(001) surface due to individual impact of slow highly charged ions. Samples were irradiated with Xe ions with charge states of $Q = 15$ to 40 at kinetic energies from 1.7 to 160 keV. The formation of nanopits at the virgin surface is observed and attributed to a defect mediated desorption process involving the removal of up to 2000 surface atoms per incident ion. The depth of the produced pits is shallow, but not limited to the first monolayer. From the variation of the ion parameters (charge state and kinetic energy) we derive a phase diagram for the structuring of the KCl(001) surface with highly charged ions.

Introduction. – Nanostructuring of surfaces by ion beam milling is a common method in research and industrial application [1–3]. These methods involve the sputtering of surface atoms due to the impacting ion beam. Typical sputtering yields are in the order of 0.1 to 10 and thus large ion fluxes need to be applied in order to mill several surface layers or large structures in a focussed ion beam setup. The sputtering yield is limited by the amount of energy which can be deposited close to the surface and thus by the stopping force of the ion. In order to increase the sputtering yield one can either increase the stopping force significantly, which is done in swift heavy ion irradiations or one uses another unique feature of heavy ions. This feature is the potential energy E_{pot} and results from the charge state of the ion. Swift heavy ion irradiations yield large sputtering yields (100-10,000) [4, 5], but are always combined with an elongated damage region in the bulk. Slow highly charged ions (HCI) instead deposit their potential energy in the range of a few keV to a few 10 keV close to the surface, i.e. within the first monolayers. This energy and the small deposition depth result in a large energy density giving rise to different kinds of nanostructures [6, 7]. Among them are nanohillocks due to a local phase transition at the surface [8, 9], etchable defect clusters [10], volcano-like structures [11, 12] and epitaxial nanopits [13, 14]. The latter are features which preserve the local lattice structure but are associated with a desorption process and corresponding desorption (or potential sputtering) yields of up to a few thousand atoms.

Due to the nature of the interaction only insulating surfaces are prone to HCI induced nanostructure formation. The potential energy is released as a result of the neutralization of the ion leading to a vast amount of electronic excitations at the surface [7,15,16]. These excitations may either be screened and dissipate rapidly in a metal or they remain at the impact site and finally couple to the lattice. The lattice excitation may then lead to local phase transformation, i.e. local melting [9, 17] or sublimation, or the formation of large defect clusters [10].

On the KBr(001) surface a defect mediated desorption process induced by slow HCI could be identified [13]. The result of a single ion impact with sufficiently high charge state is a nanopit with a depth of exactly one monolayer and a lateral extend of up to 20 nm. Corresponding desorption yields are in the order of a few 100 to 3,000 atoms/ion. The desorption results from the formation of a cluster of lattice defects, so called color centers. These color centers at high special density can lead to a collective desorption at the flat (001) surface leaving a nanopit. Here we show that the HCI related defect mediated desorption process is not unique to the KBr(001) surface, but can also be observed on the sister surface KCl(001). Similar nanopits are observed, but their depth is not limited to the first monolayer like on KBr(001). Deeper structures up to 3 monolayers are observed, whereas the depth profile depends on the ion's kinetic energy. Also the po-

tential energy threshold for the creation of these nanopits is somewhat higher than on the KBr(001) surface.

Experimental Setup. – KCl single crystals were acquired from KORTH KRISTALLE, Germany and TED PELLA, USA. Samples were cleaved in air with a razor blade parallel to the {001}-plane. Platelets with a size of approx. $10 \times 10 \times 2\,\mathrm{mm}^3$ were produced and immediately transferred into an ultra high vacuum chamber, which is maintained at $p < 5 \times 10^{-9}$ mbar during irradiation. Ion fluencies were kept between 5×10^8 and $1 \times 10^{10}\,\mathrm{cm}^{-2}$ to ensure no overlap of ion impacts. Some samples were irradiated at the Rossendorf Two-Source-Facility (2SF) and others at the new highly charged ion facility SNIPER (Surface Nanostructures by Ion's Potential Energy Release) at the ion beam center of the Helmholtz-Zentrum Dresden-Rossendorf. Samples irradiated at the 2SF were transferred in air to an ultra high vacuum atomic force microscope (AFM) from SCIENTAOMICRON (VT UHV-AFM/STM) operated in contact-mode. At SNIPER an AFM (SCIENTAOMICRON room-temperature UHV AFM/STM) is mounted within the target chamber enabling us to perform ion irradiation and AFM or STM measurements without breaking the vacuum, which we here refer as *in-vacuo*. Both AFMs use contact-mode cantilevers purchased from NANOSENSORS, USA with a nominal tip radius of 7 nm. Typical loading forces were in the range of -2 to 5 nN, corresponding to attractive and retractive regimes, respectively.
Highly charged ions are produced in both facilities in room-temperature electron beam ion traps from DREEBIT, Germany. These ion sources provide Xe ions with charge states from $Q = 1$ to 44. Ions with specific charge states are selected by an analyzing magnet or a Wien filter at the 2SF or SNIPER, respectively. Ions are decelerated by an electrostatic potential upon entry into the respective target chambers, thus we are able to adjust the ion's kinetic energy in the range of 100 to 4,500 V$\times Q$.

Experimental Results. – At SNIPER samples were analyzed with contact-mode AFM before irradiation to ensure a high quality surface after cleavage. Terraces with several micrometer in length and several hundred nanometer in width were obtained. Terraces are separated by step edges with single monolayer height. Figure 1 shows an AFM image of a KCl(001) surface after irradiation with 70 keV Xe^{35+} ions with an applied fluence of $1.4 \times 10^9\,\mathrm{cm}^{-2}$. The surface shows large terrace sizes and well aligned step edges. Single ion impacts are visible as nanopits. These pits can be found close to step edges as well as in the middle of a terrace. To evaluate the influence of the ion charge state or it's potential energy, respectively, a systematic analysis of the pit shape, i.e. it's depth and width was performed. The depth distributions of nanopits resulting from Xe^{33+}, Xe^{35+} and Xe^{40+} at similar kinetic energies of 66, 70 and 80 keV, respectively, are shown in figure 2(a). For $Q = 33$, i.e. $E_{pot} \approx 21$ keV, nanopits show a depth of one monolayer only, similar to the case of KBr

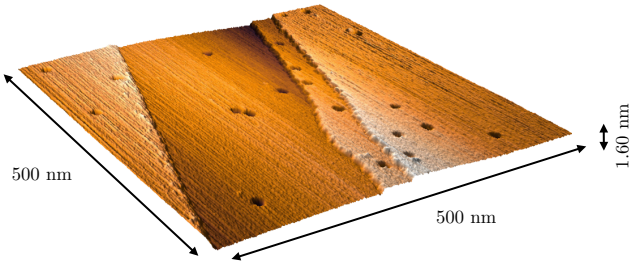

Fig. 1: (color online) 500×500 nm contact AFM image of a KCl(001) surface irradiated with Xe^{35+} at 70 keV kinetic energy. The applied ion fluence was $1.4 \times 10^9\,\mathrm{cm}^{-2}$.

[13]. Increasing the potential energy to about 25.5 keV ($Q = 35$) results in nanopits with a bimodal depth distribution. Roughly 2/3 of the pits show still a single monolayer depth, whereas 1/3 of the pits has a depth of two monolayers. At even higher potential energy of ≈ 38 keV ($Q = 40$) a bimodal distribution is obtained, which peaks at 1.5 and 2.3 monolayers.
Similar to the increase in depth pits also grow in lateral dimension when the ion charge state is increased. This is shown in figure 2(b) for the same ion parameters as discussed above. By increasing E_{pot} from 21 to 38 keV the mean pit diameter increases from about 7 to about 13 nm. From the AFM images the pit volume can be obtained directly without the assumption of a specific shape. This pit volume is shown in figure 3 as function of the potential energy of ions at different kinetic energies. The kinetic energies are 2 keV$\times Q$ (blue squares) and 4.4 keV$\times Q$ (black dots). In case of faster ions a threshold for pit formation was observed between a potential energy of 5 to 8 keV. Only if the potential energy exceeds the values of 8 keV nanopits are observed. This threshold effect is consistent with nanostructure formation on many different materials [7]. At even higher potential energies the pit volume increases slightly.
Lower kinetic energies lead to steeper increase of the pit volume with potential energy. Also, by extrapolation, a threshold in potential energy can be found at about 16-17 keV, which is significantly higher than in the case above. In the case of $Q = 35$ the data points are also indicated with the depth of the nanopits. The volume is larger for slower ions roughly by a factor 1.75, whereas pits show a mean depth of more than a single monolayer. The mean depth differs by a factor of 1.35, i.e. in case of slower ions, nanopits are not only deeper, but also larger.
The latter effect of the kinetic energy becomes obvious in figure 4, where nanopit depths for Xe^{35+} ions at two different kinetic energies are compared. As mentioned above, slower ions (70 keV) produce pits with 1-2 monolayer depth, whereas faster ions (135 keV) produce solely single monolayer deep pits. This finding can be explained by the necessary energy density for the desorption process. In case of faster ions the potential energy is deposited into deeper layers of the materials and thus the density close

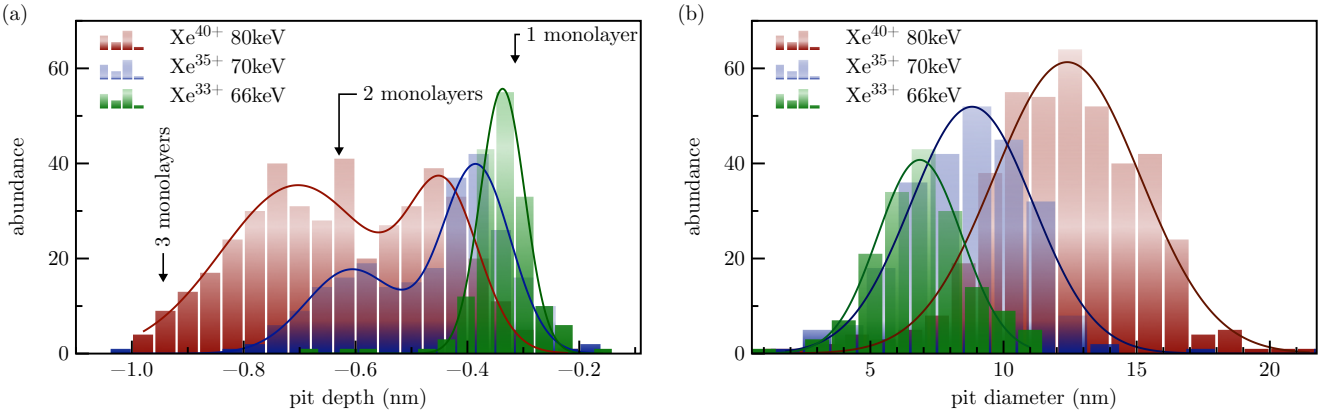

Fig. 2: (color online) (a): Depth distribution of observed nanopits. The distributions were fitted with multi-peak Gaussians. (b): Lateral size distribution of observed nanopits. The distributions were fitted with simple Gaussians.

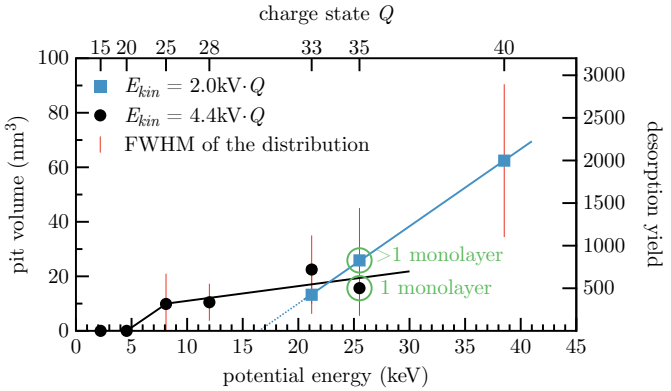

Fig. 3: (color online) Pit volume as function of ion's potential energy. The corresponding desorption yield is given on the right axis and the charge state on the top axis. The two curves correspond to two different kinetic energies. The 2 keV×Q data is extrapolated to zero volume to determine a threshold. Monolayer and mulilayer deep pits are observed for Xe^{35+} ions, depending on the kinetic energy (see fig. 4).

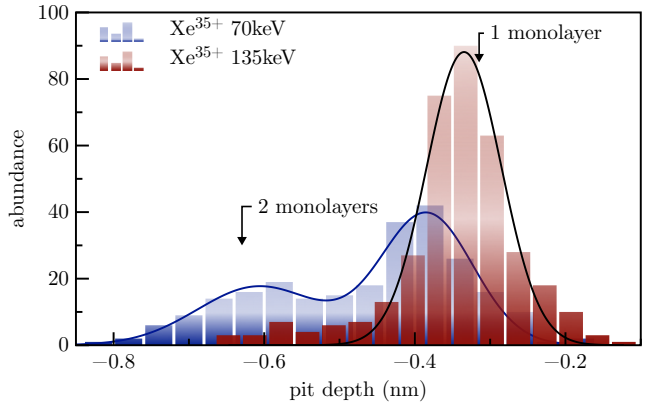

Fig. 4: (color online) Abundance of pit depth for Xe^{35+} ions at two different kinetic energies. At high E_{kin} only monolayer deep pits are observed, while slower ions produce deeper pits.

to the surface is smaller than for slower ions. Produced defects and electronic excitations can lead only to the desorption of atoms at the very surface. At higher energy densities the amount of defects and electronic excitations at the surface becomes sufficient to allow atoms from several monolayers to be removed simultaneously. This effect of the kinetic energy and consequently of the potential energy density was observed and explained by El-Said *et al.* on the CaF_2(111) surface [9].

Defect Mediated Desorption. – An highly charged ion approaching a solid surface starts to capture electrons from the surface at a large distance of about 10 a.u.. Electrons are bound to the ion in very high Rydberg states with principal quantum numbers of $n = 10 - 20$ [18–20]. The formed object is called a hollow atom or ion. Subsequent de-excitation of the hollow atom results in the emission of Auger electrons and x-rays. Upon impact of the ion electrons still bound at high Rydberg states are stripped off, because their orbitals are much larger than interatomic distances of the surface atoms. The re-charged ion now captures electrons in a multi-electron process rather than a subsequent single electron process. By these complex neutralization processes the surface is locally heavily positively charged and thus structural weakened. The ion above the surface acts as a point source for electrons with energies of 10 to a few 100 eV [21–24]. Within the surface the continuously neutralizing and de-exciting ion still emits electrons. In fact, now deep lying inner shells are filled and thus the electron energies are even higher in the order of keV.

From electron irradiation of alkali halide surfaces a layer-by-layer desorption process was identified [7, 25–28]. Impacting electrons excite bound electrons in the lattice forming an exciton which gets rapidly self-trapped due to the charge background of the ionic crystal. The self-trapped exciton (STE) is a certain form of electronic excitation, which is stable up to picoseconds. Eventually a STE will decay into two color centers, namely a F-center and a H-center. F-centers are lattice defects, where the

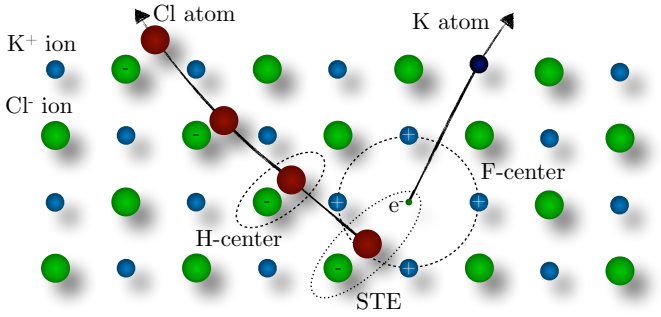

Fig. 5: (color online) The desorption process as a result of a STE decay.

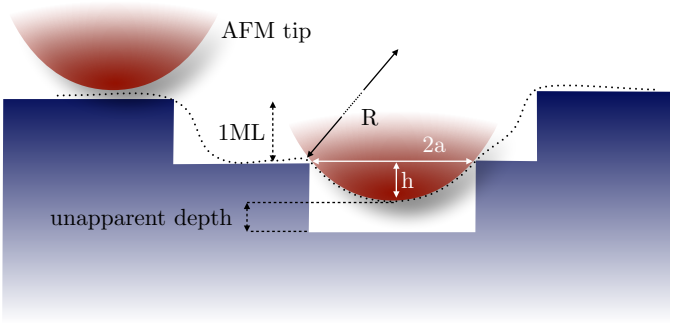

Fig. 6: (color online) Underestimation of pit depth due to the convolution of the tip profile with the pit depth profile.

halogen ion is missing and an electron is trapped at the halogen site. H-centers are quasi-molecular dimers of neutral halogen atoms and negatively charged close halogen ions (see figure 5).

F- and H-centers are mobile in the lattice and can diffuse by hopping towards the surface. At low coordinated sites at the surface these lattice defects may recombine with an alkali ion (F-centers) or simply desorb (H-centers). At a flat surface, e.g. in the middle of a large terrace, desorption may be hindered, because of the enhanced binding energy compared to a step edge. Since we still find nanopits far away from step edges and they result from a single ion impact the authors suggested on the KBr surface the formation of a large F-center cluster [13]. This cluster, called a X-center, may result in the desorption of several hundred to thousands of atoms simultaneously.

Since KBr and KCl have the same crystallographic structure and are very similar in many ways it can be assumed that a defect mediated desorption process is present here as well. However, a higher potential energy threshold must be overcome in case of KCl. Also at even higher potential energies desorption from deeper layers becomes active. Since a X-center is a hypothetical object it can also be assumed that it may have different shapes, i.e. oblate or prolate. Oblate X-centers may be present if the electron emission is dominant above the surface and prolate ones if the electron emission is strongest within the surface. These details depend heavily on the materials electron supply under the influence of the ion, i.e. the electron mobility within an electric field strength of about $10^{12}\,\mathrm{V/m}$ at a time scale of about 10 fs. It is difficult to estimate material's behaviour under these conditions. The proposed mechanism works as follows: (i) An ion with charge states $20 < Q < 35$ at intermediate kinetic energies produces a monolayer deep pit as described above. (ii) At higher potential energies the energy density increases and consequently a prolate X-center grows in size. Atoms from deeper layers can also be emitted. (iii) If now the kinetic energy increases, the energy density decreases again. Thus, the part of a X-center close to the surface will then only lead to desorption of the first layer. Deeper parts of the X-center, i.e. F-center clusters will not simultaneously desorb and just diffuse to the surface, increasing the size of the initial pit laterally.

Finally it remains open why depths of non-integer numbers of monolayers were determined. In order to measure the true depth of a nanopit one needs to take the convolution of the depth profile with the AFM's tip profile into account. In the proposed desorption mechanism not all of the atoms from the second monolayer may be desorbed (see fig. 6). In this case the AFM tip may not penetrate the second layer completely and thus an apparent depth of more than one but less than two monolayers may be measured. Tips used in this study have a nominal radius $R = 7\,\mathrm{nm}$. Assuming the tip being of spherical shape a cap with diameter $2a$ and a cap height h can be assumed. The radius a, which a spherical pit must maintain in order for the tip to penetrate completely by the height h is given by $a = \sqrt{2Rh - h^2}$. For a pit depth h of one monolayer (0.32 nm), it's lateral dimension must be larger than 4.2 nm to be measured correctly. For a two-monolayer-deep pit, it's lateral dimension must even exceed 5.9 nm. Vice versa a shift of the mean depth by 0.5 monolayers corresponds to a lateral extend of the desorbed region from the second layer of 2.9 nm. If a two-monolayer-deep pit is not entirely of cylindrical shape, i.e. only parts of the second layer are desorbed, it's apparent depth can adapt values between 1 and 2 monolayers (see fig. 3). The same holds for even deeper structures. This also means that the desorption yield of multi-layer-deep pits is underestimated in the present study.

Nanopits of different shapes were observed for certain ion parameters, i.e. potential and kinetic energy. If the ion charge state or the kinetic energy is too low no pits are observed and the surface appears unchanged. Combinations of both ion parameters are shown in green in figure 7 where nanopits were found. A kinetic energy dependent threshold is determined in the range of 0-100 keV and xenon charge states between 15 and 33. This 'phase diagram' is similar to the one reported for KBr [14] justifying once more the adaption of a defect mediated desorption process.

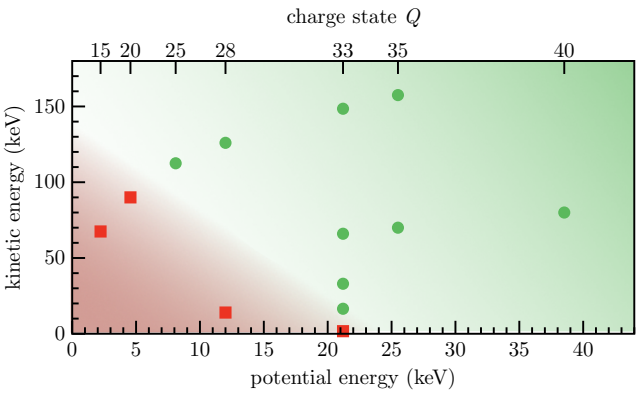

Fig. 7: (color online) Phase diagram for KCl(001) nanostructuring by slow HCI. An estimated area where no pits are expected is colored in red (data points as red squares), an area where pits were observed and expected is colored in green (data points as green dots).

Conclusions. – We showed that individual highly charged ion impact leads to nanopit formation with associated desorption yields of up to 2,000 atoms/ion on KCl(001). Pits are similar to single-monolayer-deep structures observed on KBr(001), but show a depth distribution indicating desorption also from deeper layers. A clear potential energy dependence of the desorption yield is presented. Additionally high kinetic energy alters the depth distribution of ion induced defects and thus reduces the efficiency of the desorption process. A phase diagram for the structuring of the KCl(001) surface with highly charged ions is deduced.

* * *

Support by the Deutsche Forschungsgemeinschaft (project no. HE 6174/1-1) is gratefully acknowledged.

REFERENCES

[1] Harriott L. R., *J. Vac. Sci. Technol. B Microelectron. Nanom. Struct.*, **4** (1986) 181.
[2] Reyntjens S. and Puers R., *J. Micromechanics Microengineering*, **11** (2001) 287.
[3] Valbusa U., Boragno C. and Mongeot F. B. D., *J. Phys. Condens. Matter*, **14** (2002) 8153.
[4] Chadderton L. T., *Radiat. Meas.*, **36** (2003) 13.
[5] Toulemonde M., Assmann W., Trautmann C. and Grüner F., *Phys. Rev. Lett.*, **88** (2002) 057602.
[6] Aumayr F., Facsko S., El-Said A. S., Trautmann C. and Schleberger M., *J. Phys. Condens. Matter*, **23** (2011) 393001.
[7] Wilhelm R. a., El-Said A. S., Krok F., Heller R., Gruber E., Aumayr F. and Facsko S., *Prog. Surf. Sci.*, **90** (2015) 377.
[8] El-Said A., Meissl W., Simon M., Crespo López-Urrutia J., Lemell C., Burgdörfer J., Gebeshuber I., Winter H., Ullrich J., Trautmann C., Toulemonde M. and Aumayr F., *Nucl. Instruments Methods Phys. Res. Sect. B Beam Interact. with Mater. Atoms*, **258** (2007) 167.
[9] El-Said A. S., Heller R., Meissl W., Ritter R., Facsko S., Lemell C., Solleder B., Gebeshuber I. C., Betz G., Toulemonde M., Möller W., Burgdörfer J. and Aumayr F., *Phys. Rev. Lett.*, **100** (2008) 237601.
[10] El-Said A. S., Wilhelm R. A., Heller R., Facsko S., Lemell C., Wachter G., Burgdörfer J., Ritter R. and Aumayr F., *Phys. Rev. Lett.*, **109** (2012) 117602.
[11] Tona M., Fujita Y., Yamada C. and Ohtani S., *Phys. Rev. B*, **77** (2008) 155427.
[12] Ritter R., Wilhelm R. A., Ginzel R., Kowarik G., Heller R., El-Said A. S., Papaléo R. M., Rupp W., Crespo López-Urrutia J. R., Ullrich J., Facsko S. and Aumayr F., *EPL (Europhysics Lett.*, **97** (2012) 13001.
[13] Heller R., Facsko S., Wilhelm R. A. and Möller W., *Phys. Rev. Lett.*, **101** (2008) 096102.
[14] Facsko S., Heller R., El-Said A. S., Meissl W. and Aumayr F., *J. Phys. Condens. Matter*, **21** (2009) 224012.
[15] Arnau A., Aumayr F., Echenique P., Grether M., Heiland W., Limburg J., Morgenstern R., Roncin P., Schippers S., Schuch R., Stolterfoht N., Varga P., Zouros T. and Winter H., *Surf. Sci. Rep.*, **27** (1997) 113.
[16] Aumayr F. and Winter H., *Philos. Trans. R. Soc. A Math. Phys. Eng. Sci.*, **362** (2004) 77.
[17] Lemell C., El-Said A., Meissl W., Gebeshuber I., Trautmann C., Toulemonde M., Burgdörfer J. and Aumayr F., *Solid. State. Electron.*, **51** (2007) 1398.
[18] Burgdörfer J., Lerner P. and Meyer F. W., *Phys. Rev. A*, **44** (1991) 5674.
[19] Bárány A. and Setterlind C. J., *Nucl. Instruments Methods Phys. Res. Sect. B Beam Interact. with Mater. Atoms*, **98** (1995) 184.
[20] Ducrée J. J., Casali F. and Thumm U., *Phys. Rev. A*, **57** (1998) 338.
[21] Kurz H., Aumayr F., Lemell C., Töglhofer K. and Winter H., *Phys. Rev. A*, **48** (1993) 2182.
[22] Aumayr F., Kurz H., Schneider D., Briere M. A., McDonald J. W., Cunningham C. E. and Winter H., *Phys. Rev. Lett.*, **71** (1993) 1943.
[23] Aumayr F. and Winter H. P., *Slow Heavy-Particle Induced Electron Emission from Solid Surfaces* Vol. 225 of *Springer Tracts in Modern Physics* (Springer Berlin Heidelberg, Berlin, Heidelberg) 2007.
[24] Meissl W., Winklehner D., Aumayr F., Simon M. C., Ginzel R., López-Urrutia J. R. C., Ullrich J., Solleder B., Lemell C. and Burgdörfer J., *e-Journal Surf. Sci. Nanotechnol.*, **6** (2008) 54.
[25] Such B., Kolodziej J., Czuba P., Piatkowski P., Struski P., Krok F. and Szymonski M., *Phys. Rev. Lett.*, **85** (2000) 2621.
[26] Bennewitz R., Schär S., Barwich V., Pfeiffer O., Meyer E., Krok F., Such B., Kolodzej J. and Szymonski M., *Surf. Sci.*, **474** (2001) L197.
[27] Kolodziej J., Such B., Czuba P., Krok F., Piatkowski P., Struski P., Szymonski M., Bennewitz R., Schär S. and Meyer E., *Surf. Sci.*, **482-485** (2001)

903.
[28] Szymonski M., Droba A., Struski P. and Krok F., *Low Temp. Phys.*, **38** (2012) 774.